DOI: 10.2352/ISSN.2470-1173.2016.2.VIPC-228

Guided Filter Demosaicking For Fourier Spectral Filter Array

Jie Jia, Chuan Ni, Andrew Sarangan, and Keigo Hirakawa; University of Dayton; 300 College Park, Dayton, OH 45469, USA

Abstract

We recently introduced a spectral filter array design for single-shot multispectral imaging that is based on Fourier transform spectroscopy. In this article, we investigate feasibility of guided filter demosaicking for our SFA design.

Introduction

Conventional colorimetric image sensors capture red, green, and blue samples. Multispectral image (MSI) system capture more than three spectral components with the goal to detect, identify, or track objects based on their spectral characteristics. Drawing on the success of the color filter array (CFA) in conventional cameras, spectral filter arrays (SFA) have been proposed as a single-shot MSI solution [1, 2, 3, 6, 5, 4]. Specifically, N predetermined spectral filters are spatially multiplexed over the pixel array. An interpolation step (known as *demosaicking*) is needed to recover a full resolution multispectral image. Most existing SFA designs use narrowband filters that make measurements over a small interval of wavelength/wavenumber ranges. However, question remains as to whether narrowband samples faithfully represent spectral features such as the wavelengths at which spectral peaks and attenuation occur.

We recently proposed a novel MSI based on Fourier transform spectroscopy [10], aimed at presenting the spectral features of interest with fewest spectral samples. Appealing to the fact that each interferometric measurement is equivalent to taking inner product between a sinusoidal function and the full spectrum in the wavenumber domain, we replaced the narrowband filter with broadband filters whose transmittance follows sinusoidal shape, a process by which we obtain interferometric measurements at every pixel. We proved that Fourier spectroscopy-based MSI preserves spectral features more accurately than the narrowband MSI [11], and proposed spatial arrangements of SFA using these sinusoidal filters (hereafter referred to as Fourier SFA) [10]. In our earlier work, less emphasis was placed on the demosaicking procedure. In this paper, we investigate the feasibility of repurposing demosaicking method in [5] for the Fourier SFA pattern in [10].

Fourier Spectral Filter Array Design

Spectral imagery is typically represented as a three dimensional cube, where two dimensions are associated to pixel coordinates and one dimension is in wavelength/wavenumber. Figure 1(a) illustrates a typical hyperspectral image in space-wavenumber representation $\widehat{X}(\boldsymbol{n},\sigma)$, where $\boldsymbol{n}\in\mathbb{Z}^2$ is the pixel index and σ is the wavenumber index. Since $\widehat{X}(\boldsymbol{n},\sigma)$ is a high bandwidth data for all $\sigma\in(\sigma_{min},\sigma_{max})$ values, it is difficult to determine which narrowband filter sets should be chosen for MSI. By comparison, the interferometric measurements in Fourier transform spectroscopy are sampled in the optical path difference (OPD) domain. A forword Fourier transform is applied to the OPD samples to yield spectral data in wavelength/wavenumber domain. Figure 1(b) shows hyperspectral image in space-OPD domain:

$$X(\boldsymbol{n},\zeta)=\int_{\mathbb{R}}\widehat{X}(\boldsymbol{n},\sigma)e^{-j2\pi\zeta\sigma}d\sigma, \tag{1}$$

which has the same pixel index $\boldsymbol{n}$ and the corresponding OPD index ζ. The representation in $X(\boldsymbol{n},\zeta)$ enjoy a rapid decay in signal strength as ζ increases. This phenomenon suggests that sampling in OPD domain would result in optimal MSI capture with minimal loss in spectral fidelity. In [10], we proposed a five band SFA pattern shown in Figure 2(a) designed to minimize the risk of aliasing stemming from spatial-spectral under-sampling. The measurements taken by these filters can be represented by

$$\begin{bmatrix}A(\boldsymbol{n})\\B(\boldsymbol{n})\\C(\boldsymbol{n})\\D(\boldsymbol{n})\\E(\boldsymbol{n})\end{bmatrix}=M\begin{bmatrix}X(\boldsymbol{n},\zeta_1)\\X(\boldsymbol{n},\zeta_2)\\X(\boldsymbol{n},\zeta_3)\\X(\boldsymbol{n},\zeta_4)\\X(\boldsymbol{n},\zeta_5)\end{bmatrix},$$

$$M=\begin{bmatrix}1&0&0&0&0\\ \delta_B(\zeta_1)&\delta_B(\zeta_2)&\delta_B(\zeta_3)&\delta_B(\zeta_4)&\delta_B(\zeta_5)\\ \delta_C(\zeta_1)&\delta_C(\zeta_2)&\delta_C(\zeta_3)&\delta_C(\zeta_4)&\delta_C(\zeta_5)\\ \delta_D(\zeta_1)&\delta_D(\zeta_2)&\delta_D(\zeta_3)&\delta_D(\zeta_4)&\delta_D(\zeta_5)\\ \delta_E(\zeta_1)&\delta_E(\zeta_2)&\delta_E(\zeta_3)&\delta_E(\zeta_4)&\delta_E(\zeta_5)\end{bmatrix}, \tag{2}$$

where $\{A(\boldsymbol{n}),...,E(\boldsymbol{n})\}$ are the sensor measurements from filters A-E, $X(\boldsymbol{n},\zeta_k)$ are the OPD samples, and $\{\delta_B(\zeta_k),...,\delta_E(\zeta_k)\}$ represents the contribution of OPD sample $X(\boldsymbol{n},\zeta_k)$ to $\{B(\boldsymbol{n}),...,E(\boldsymbol{n})\}$, respectively. Specifically, a spectral image captured by this SFA results in SFA-sampled data

$$Z(\boldsymbol{n})=\begin{cases}A(\boldsymbol{n}) & \text{if } \boldsymbol{n}\in\Lambda_A\\ B(\boldsymbol{n}) & \text{if } \boldsymbol{n}\in\Lambda_B\\ C(\boldsymbol{n}) & \text{if } \boldsymbol{n}\in\Lambda_C\\ D(\boldsymbol{n}) & \text{if } \boldsymbol{n}\in\Lambda_D\\ E(\boldsymbol{n}) & \text{if } \boldsymbol{n}\in\Lambda_E\end{cases} \tag{3}$$

where $\Lambda_A,\ldots,\Lambda_E\subset\mathbb{Z}^2$ correspond to locations of filters $A-E$ in Figure 2(a). The key contribution of our prior work in [10] is the way to choose $\{\delta_B(\zeta_k),...,\delta_E(\zeta_k)\}$ in (2) and $\Lambda_A,\ldots,\Lambda_E\subset\mathbb{Z}^2$ in (3) such that the risks of aliasing is small. Indeed, the composite image $Z(\boldsymbol{n})$ yields spatial Fourier decomposition that approximately decouples OPD samples, as shown in Figure 2(b).

Guided Filter Demosaicking and Spectrum Recovery

The authors of [5] proposed a demosaicking method called guided filter demosaicking used on the narrowband SFA pattern

DOI: 10.2352/ISSN.2470-1173.2016.2.VIPC-228

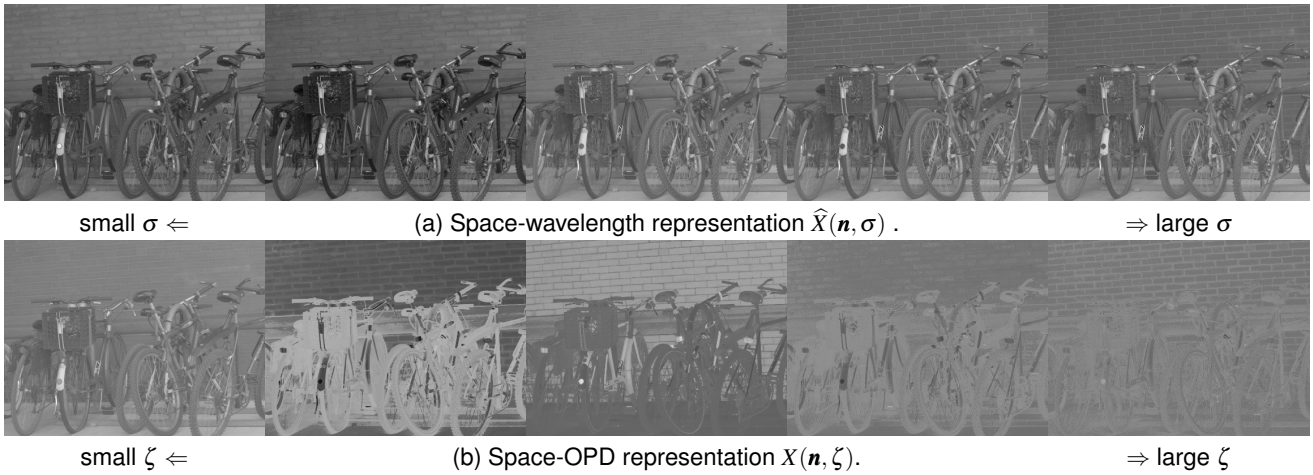

Figure 1. *Hyperspectral image signal in various forms of representation.*

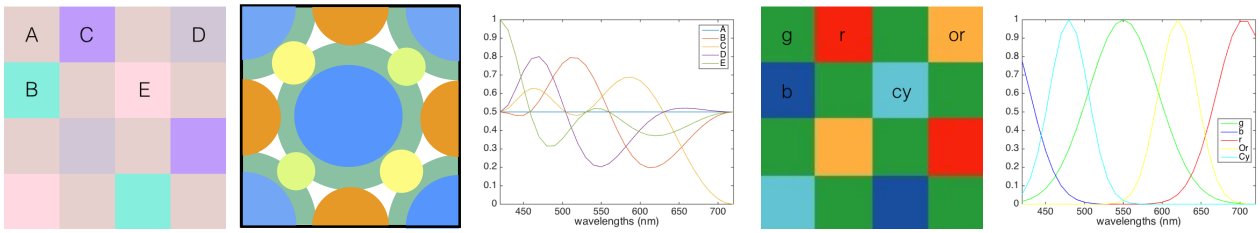

Figure 2. *(a) Fourier SFA [10]. (b) Spatial Fourier transform of the Fourier SFA-captured sensor data. The color represents various OPD measurements. (c) Spectral transmittance of filters in (a). (d) Narrowband SFA in [6]. (e) Spectral transmittance of narrowband filters in (d).*

in [6] shown in Figure 2(d). In this paper, we exploit the fact that the resultant Fourier SFA pattern share similarity with the narrowband SFA of [6].

Specifically the proposed Fourier SFA pattern has 5 broadband filters spatially arranged in the same pixel positions as the narrowband SFA, even through the pattern was designed based on its spatial Fourier decomposition as illustrated by Figure 2(b). The spectral transmittance is quite different, however. Filters *B*-*E* in Figure 2(c) are linear combinations of a few OPD samples. We investigate the feasibility of the repurposing demosaicking algorithm in [5] intended for a SFA pattern in [6] to demosaick the proposed Fourier SFA pattern in [10] to recover complete measurements $\{A(\boldsymbol{n}),...,E(\boldsymbol{n})\}$ from $Z(\boldsymbol{n})$. We subsequently use $\{A(\boldsymbol{n}),...,E(\boldsymbol{n})\}$ to reconstruct OPD samples $X(\boldsymbol{n},\zeta)$, and then the spectrum $\widehat{X}(\boldsymbol{n},\sigma)$. In our pattern in [10], filter A is designed as a panchromatic filter shown in Figure 2(c). Because the filter A spans half of the sampling density in the Fourier SFA pattern, the filter A-sampled data is chosen to generate the guide image. In this original form as developed in [5], the guide image-based demosaicking result from filter B takes the form

$$B(\boldsymbol{n}) = p(\boldsymbol{n})A(\boldsymbol{n}) + q(\boldsymbol{n}), \tag{4}$$

where $B(\boldsymbol{n})$ is the demosaicking output, $A(\boldsymbol{n}) = X(\boldsymbol{n},\zeta_1)$ is the intensity of the guide image, and $(p(\boldsymbol{n}),q(\boldsymbol{n}))$ are demosaicking coefficients. $\{C(\boldsymbol{n}),...,E(\boldsymbol{n})\}$ are recovered similarly. The coefficients $(p(\boldsymbol{n}),q(\boldsymbol{n}))$ are determined by minimizing reconstruction errors of the known pixel values in Λ_B within a neighborhood W_n near $\boldsymbol{n}$ where B-filtered measurement are made:

$$(p(\boldsymbol{n}),q(\boldsymbol{n})) = \arg\min_{p,q} \sum_{\boldsymbol{m}\in W_{\boldsymbol{n}}\cap\Lambda_B} (p\cdot A(\boldsymbol{m}) + q - Z(\boldsymbol{m}))^2 + \varepsilon p^2 \tag{5}$$

where ε is a smoothing parameter. However, (2) suggests that $A(\boldsymbol{n}) = X(\boldsymbol{n},\zeta_1)$ is already mixed into $\{B(\boldsymbol{n}),...,E(\boldsymbol{n})\}$:

$$B(\boldsymbol{n}) = \delta_B(\zeta_1)A(\boldsymbol{n}) + \delta_B(\zeta_2)X(\boldsymbol{n},\zeta_2) + ... + \delta_B(\zeta_5)X(\boldsymbol{n},\zeta_5). \tag{6}$$

Hence we propose to modify the guide image-based demosaicking as follows:

$$(\widetilde{p}(\boldsymbol{n}),\widetilde{q}(\boldsymbol{n})) = \arg\min_{\widetilde{p},\widetilde{q}} \sum_{\boldsymbol{m}\in W_{\boldsymbol{n}}} ((\widetilde{p} + \delta_B(\zeta_1))\cdot A(\boldsymbol{m}) + \widetilde{q} - Z(\boldsymbol{m}))^2 + \varepsilon\widetilde{p}^2, \tag{7}$$

This essentially subtracts away $\delta_B(\zeta_1)A(\boldsymbol{n})$ from the filter measurement $Z(\boldsymbol{n})$—$\widetilde{p}^2$ should be smaller than p^2, and the demosaicking coefficients should be more accurate and stable as a result. The demosaicked image is:

$$\widetilde{B}(\boldsymbol{n}) = \widetilde{p}(\boldsymbol{n})A(\boldsymbol{n}) + \widetilde{q}(\boldsymbol{n}), \tag{8}$$

which is a proxy for a guide image-based estimate for $B(\boldsymbol{n}) - \delta_B(\zeta_1)A(\boldsymbol{n})$. The same process is also applied to $\{\widetilde{C}(\boldsymbol{n}),...,\widetilde{E}(\boldsymbol{n})\}$.

DOI: 10.2352/ISSN.2470-1173.2016.2.VIPC-228

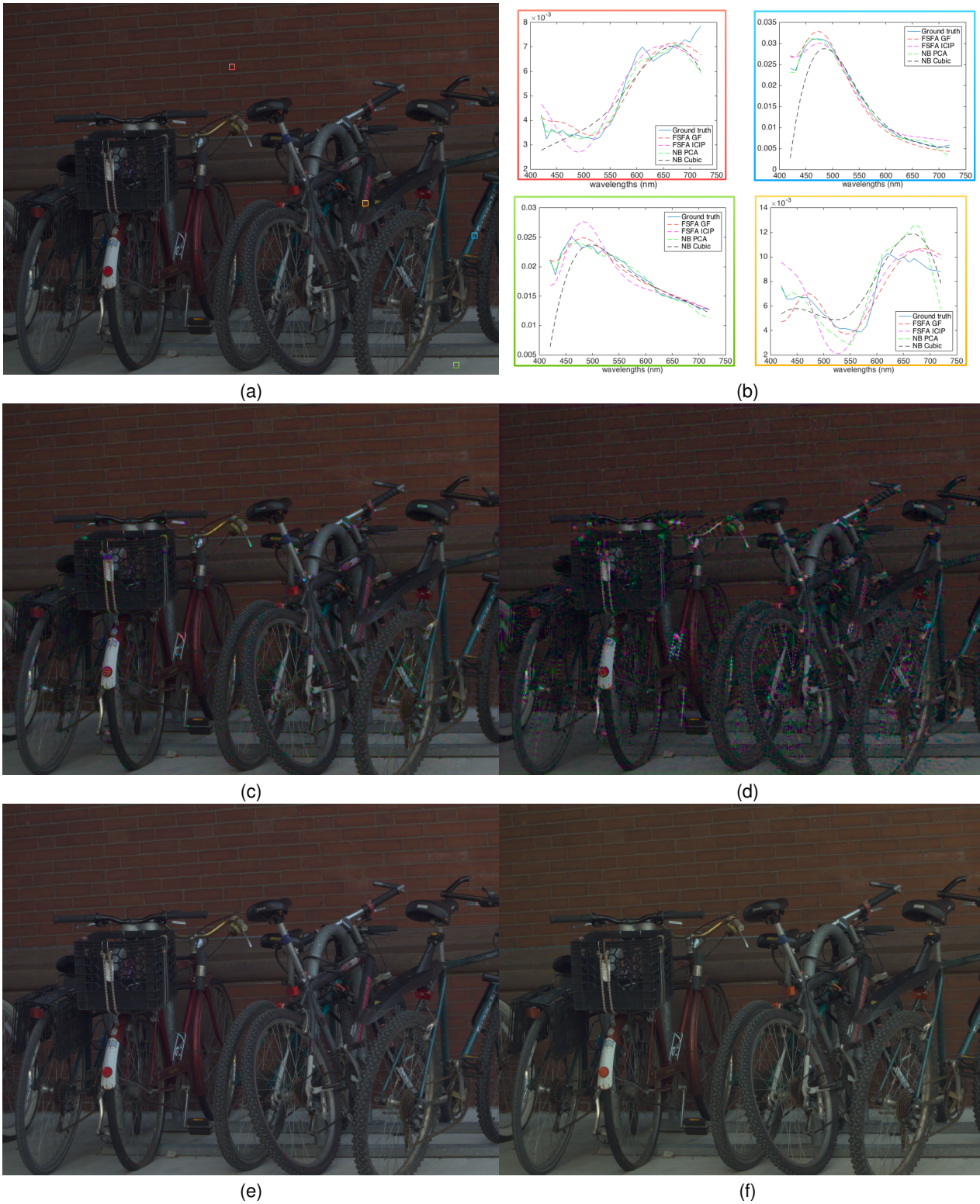

Figure 3. *Color images rendered from hyperspectral data. (a) and (b): ground truth and the spectrum reconstruction compassion, what the color boxes in (a) indicate where they are sampled. The blue line is ground truth; the red line is the Fourier SFA using demosaicking methods in [5] ; the pink line is Fourier SFA using demosaicking methods in [10]; the green line is SFA in [6] using PCA spectrum recovery; and the black line is SFA in [6] using cubic interpolation spectrum recovery. (c) and (d): reconstructed from Fourier SFA using demosaicking methods in [5] and [10], respectively. (e) and (f): reconstructed from SFA in [6] using demosicking method in [5] with PCA and cubic interpolation spectrum recovery, respectively.*

DOI: 10.2352/ISSN.2470-1173.2016.2.VIPC-228

Mean squared errors (MSE) and execution times of of recovered hyperspectral image averaged over 73 image set in [9].

SFA Pattern	Fourier SFA [10]		Narrowband SFA [6]	
Demosaicking Method	Guided Filter [5]	Demodulation [10]	Guided Filter [5]	
Spectrum Recovery Method	Fourier Transform [10]		PCA [8]	Cubic Interpolation
Average MSE	**7.23E-48**	1.00E-47	7.45E-48	9.84E-48
Min MSE	**3.23E-49**	6.12E-49	6.45E-49	7.80E-49
Max MSE	1.51E-46	1.52E-46	**1.16E-46**	1.96E-46
Stdev MSE	1.82E-47	2.07E-47	1.40E-47	2.34E-47
Average execution time (sec)	600	400	162000	1800

Combining 2 and 7, OPD samples $X(\boldsymbol{n},\zeta)$ and demosaicked image $\{A(\boldsymbol{n}),\widetilde{B}(\boldsymbol{n}),\widetilde{C}(\boldsymbol{n}),\widetilde{D}(\boldsymbol{n}),\widetilde{E}(\boldsymbol{n})\}$ are related by:

$$\begin{bmatrix} A(\boldsymbol{n}) \\ \widetilde{B}(\boldsymbol{n}) \\ \widetilde{C}(\boldsymbol{n}) \\ \widetilde{D}(\boldsymbol{n}) \\ \widetilde{E}(\boldsymbol{n}) \end{bmatrix} = \begin{bmatrix} A(\boldsymbol{n}) \\ B(\boldsymbol{n})-\delta_B(\zeta_1)A(\boldsymbol{n}) \\ C(\boldsymbol{n})-\delta_C(\zeta_1)A(\boldsymbol{n}) \\ D(\boldsymbol{n})-\delta_D(\zeta_1)A(\boldsymbol{n}) \\ E(\boldsymbol{n})-\delta_E(\zeta_1)A(\boldsymbol{n}) \end{bmatrix} = N \begin{bmatrix} X(\boldsymbol{n},\zeta_1) \\ X(\boldsymbol{n},\zeta_2) \\ X(\boldsymbol{n},\zeta_3) \\ X(\boldsymbol{n},\zeta_4) \\ X(\boldsymbol{n},\zeta_5) \end{bmatrix},$$

where

$$N = \begin{bmatrix} 1 & 0 & 0 & 0 & 0 \\ 0 & \delta_B(\zeta_2) & \delta_B(\zeta_3) & \delta_B(\zeta_4) & \delta_B(\zeta_5) \\ 0 & \delta_C(\zeta_2) & \delta_C(\zeta_3) & \delta_C(\zeta_4) & \delta_C(\zeta_5) \\ 0 & \delta_D(\zeta_2) & \delta_D(\zeta_3) & \delta_D(\zeta_4) & \delta_D(\zeta_5) \\ 0 & \delta_E(\zeta_2) & \delta_E(\zeta_3) & \delta_E(\zeta_4) & \delta_E(\zeta_5) \end{bmatrix}, \quad (9)$$

and $\delta_B(\zeta_k)$ represents the contribution of OPD sample $X(\boldsymbol{n},\zeta_k)$ in $\widetilde{B}(\boldsymbol{n})$, etc. We recover the OPD samples $\{X(\boldsymbol{n},\zeta_1),...,X(\boldsymbol{n},\zeta_5)\}$ by linearly uncombining the OPDs in demosaicked images $\{A(\boldsymbol{n}),\widetilde{B}(\boldsymbol{n}),\widetilde{C}(\boldsymbol{n}),\widetilde{D}(\boldsymbol{n}),\widetilde{E}(\boldsymbol{n})\}$ by:

$$\begin{bmatrix} X(\boldsymbol{n},\zeta_1) \\ X(\boldsymbol{n},\zeta_2) \\ X(\boldsymbol{n},\zeta_3) \\ X(\boldsymbol{n},\zeta_4) \\ X(\boldsymbol{n},\zeta_5) \end{bmatrix} = N^{-1} \begin{bmatrix} A(\boldsymbol{n}) \\ \widetilde{B}(\boldsymbol{n}) \\ \widetilde{C}(\boldsymbol{n}) \\ \widetilde{D}(\boldsymbol{n}) \\ \widetilde{E}(\boldsymbol{n}) \end{bmatrix}. \quad (10)$$

Finally, the space-wavenumber image $\widehat{X}(\boldsymbol{n},\sigma)$ is reconstructed by taking Fourier transform of the recoverd OPD samples:

$$\begin{aligned} \widehat{X}(\boldsymbol{n},\sigma) &= \int_{\mathbb{R}} X(\boldsymbol{n},\zeta)e^{j2\pi\zeta\sigma}d\zeta \\ &\approx \int_{\mathbb{R}} \Delta\zeta \sum_k X(\boldsymbol{n},\zeta_k)\delta(\zeta-\zeta_k)e^{j2\pi\zeta\sigma}d\zeta \quad (11) \\ &= \Delta\zeta X(\boldsymbol{n},\zeta_1) + 2\Delta\zeta \sum_k X(\boldsymbol{n},\zeta_k)\cos(2\pi\zeta_k\sigma), \end{aligned}$$

where $\Delta\zeta$ is the spacing between OPD samples ζ_k and ζ_{k+1}.

Fast Rendering of Color Image

Although the goal of proposed Fourier SFA scheme is to reconstruct the hyperspectral image, RGB image can be recovered with minimal computation. Recall tristimulus values $\{r(\boldsymbol{n}),g(\boldsymbol{n}),b(\boldsymbol{n})\}$ is computed by an inner product between the spectrum $\widehat{X}(\boldsymbol{n},\sigma)$ and the color matching functions $\{\bar{r}(\sigma),\bar{g}(\sigma),\bar{b}(\sigma)\}$:

$$\begin{bmatrix} r(\boldsymbol{n}) \\ g(\boldsymbol{n}) \\ b(\boldsymbol{n}) \end{bmatrix} = \int_{\mathbb{R}} \begin{bmatrix} \bar{r}(\sigma) \\ \bar{g}(\sigma) \\ \bar{b}(\sigma) \end{bmatrix} \widehat{X}(\boldsymbol{n},\sigma)d\sigma. \quad (12)$$

Substituting (10) and (11),

$$\begin{aligned} \begin{bmatrix} r(\boldsymbol{n}) \\ g(\boldsymbol{n}) \\ b(\boldsymbol{n}) \end{bmatrix} &= \Delta\zeta \int_{\mathbb{R}} \begin{bmatrix} \bar{r}(\sigma) \\ \bar{g}(\sigma) \\ \bar{b}(\sigma) \end{bmatrix} \begin{bmatrix} 1 \\ 2\cos(2\pi\zeta_2\sigma) \\ \vdots \\ 2\cos(2\pi\zeta_5\sigma) \end{bmatrix}^T N^{-1} \begin{bmatrix} A(\boldsymbol{n}) \\ \widetilde{B}(\boldsymbol{n}) \\ \widetilde{C}(\boldsymbol{n}) \\ \widetilde{D}(\boldsymbol{n}) \\ \widetilde{E}(\boldsymbol{n}) \end{bmatrix} d\sigma \\ &= T \begin{bmatrix} A(\boldsymbol{n}) \\ \widetilde{B}(\boldsymbol{n}) \\ \widetilde{C}(\boldsymbol{n}) \\ \widetilde{D}(\boldsymbol{n}) \\ \widetilde{E}(\boldsymbol{n}) \end{bmatrix} \quad (13) \end{aligned}$$

where $T \in \mathbb{R}^{3\times 5}$,

$$T = \Delta\zeta \left(\int_{\mathbb{R}} \begin{bmatrix} \bar{r}(\sigma) \\ \bar{g}(\sigma) \\ \bar{b}(\sigma) \end{bmatrix} \begin{bmatrix} 1 \\ cos(2\pi\zeta_2\sigma) \\ \vdots \\ cos(2\pi\zeta_5\sigma) \end{bmatrix}^T d\sigma \right) N^{-1}. \quad (14)$$

The multiplication by $T \in \mathbb{R}^{3\times 5}$ is a minimal computational overhead, far less demanding than reconstructing the full spectrum.

Simulated Experimental Results

We compared demosaicking of [5] repurposed for Fourier SFA to a simpler demodulation-based demosaicking used in [10]. For simulation, we used hyperspectral data in [9] comprised of 31 narrowband measurements in 420nm-720nm range over 1040×1392 pixels. The color artifacts are observed in the demosaicking result of [10] in Figure 3(d) are significantly reduced by the guided filter demosaicking result in Figure 3(c). As shown in Table 1, the mean squared error (MSE) values computed in the wavelength domain also suggest significant improvement. We also compared against the narrowband SFA in [6] with the same guided filter demosaicking in [5], where the spectrum was reconstructed using cubic interpolation through the filters' center wavelength shown in Figure 3(f) and by nonnegative projection onto 8 principal component analysis (PCA) vectors (as described in [8] which the authors of [6] follow) trained over the data set in [9] shown in Figure 3(e). The narrowband SFA reconstruction based on cubic interpolation was far worse than the proposed combination of Fourier SFA and guided filter demosaicking, even though the complexities are comparable to ours. The quality of hyperspectral image reconstructed from narrowband SFA with nonnegative PCA projection was comparable to the proposed Fourier SFA scheme, though the method in [8] was far more complex.

DOI: 10.2352/ISSN.2470-1173.2016.2.VIPC-228

The last row of Table 1 summarizes the execution time for the algorithms considered using Matlab 2015a running on Mac Pro (3.7 GHz Quad-Core Intel Xeon E5 and 64GB RAM). The complexity of proposed configuration (combining Fourier SFA with demosaicking in [5]) is comparable to the Fourier SFA demosaicking of [10]. The proposed configuration is faster than the combination of SFA in [6], guide image demosaicking in [5], and cubic interpolation. The nonnegative PCA projection method in [8] is clearly the computational bottleneck. Contrast this also to the fast color image rendering technique proposed in (13) and (14), which averages 10 second execution time.

Conclusions

We proposed to combine demosaicking method of [6] with Fourier SFA pattern [10]. It improved the accuracy of spectrum reconstruction over the demosaicking used in [10] as well as narrowband SFA design of [6]. The speed of the hyperspectral image recovery was significantly faster because of the linear reconstruction of $\widehat{X}(\boldsymbol{n},\sigma)$ from demosaicked images.

Acknowledgments

This work was funded in part by the National Science Foundation under grant No. 1307904.

References

[1] J.M. Eichenholz, N. Barnett, Y. Juang, D. Fish, S. Spano, E. Lindsley, and D.L. Farkas. Real time megapixel multispectral bioimaging. In *Proc. SPIE*, volume 7568, 2010.

[2] G.A. Baone and H. Qi. Demosaicking methods for multispectral cameras using mosaic focal plane array technology. In *Proceedings of SPIE*, volume 6062, page 60620A, 2006.

[3] L. Miao, H. Qi, and W.E. Snyder. A generic method for generating multispectral filter arrays. In *Image Processing, 2004. ICIP'04. 2004 International Conference on*, volume 5, pages 3343–3346. IEEE, 2004.

[4] Y. Monno, M. Tanaka, and M. Okutomi. Multispectral demosaicking using adaptive kernel upsampling. In *Image Processing (ICIP), 2011 18th IEEE International Conference on*, pages 3157–3160. IEEE, 2011.

[5] Y. Monno, M. Tanaka, and M. Okutomi. Multispectral demosaicking using guided filter. *Proceedings of IS&T/SPIE Electronic Imaging (EI2012)*, 8299:82990–1, 2012.

[6] Y. Monno, T. Kitao, M. Tanaka, and M. Okutomi. Optimal spectral sensitivity functions for a single-camera one-shot multispectral imaging system. In *Image Processing (ICIP), IEEE International Conference on*, 2012.

[7] K. Hirakawa and K. J Barnard. Fourier spectral filter array design for multispectral image recovery. In *Imaging Systems and Applications*, pages IM1C–5. Optical Society of America, 2014.

[8] J.I. Park, M.H. Lee, M.D. Grossberg, and S.K. Nayar. Multispectral imaging using multiplexed illumination. In *Computer Vision, 2007. ICCV 2007. IEEE 11th International Conference on*, pages 1–8. IEEE, 2007.

[9] A. Chakrabarti and T. Zickler. Statistics of Real-World Hyperspectral Images. In *Proc. IEEE Conf. on Computer Vision and Pattern Recognition (CVPR)*, pages 193–200, 2011.

[10] J. Jia and K. Hirakawa. Single-shot Fourier Transform Multispectroscopy. In *Image Processing (ICIP), 2015 IEEE International Conference*.

[11] J. Jia, C. Ni, A. M. Sarangan, and K. Hirakawa. Fourier multispectral imaging. In *OSA Optics Express*, 2015.

Author Biography

Jie Jia received his BS in Communication Engineer from the Beijing University of Posts and Communication (2009) and his master degree in Electronic Engineer from University of Dayton (2011). Since 2012, he has joined the Intelligent Signal Systems Laboratory at the University of Dayton as a PhD candidate. His work has focused on multispectral imaging.

Chuan Ni received his BS in Optics from the Nanjing University of Science and Technology (2011) and his MS in Electro-Optics from the University of Dayton (2014). Since 2014, he has joined at Nano-Fab Lab in University of Dayton as a PhD student. His work has focused on thin films, filter design and fabrication. He is a member of SPIE.

Andrew Sarangan is a Professor and Associate Director of the Electro-Optics Graduate Program at the University of Dayton, Ohio. He received his BASc and PhD degrees from the University of Waterloo in Canada in 1991 and 1997 respectively. His research areas are in infrared photodetector technologies, polarimetric imaging, nanofabrication, nanostructured thin films and computational electromagnetics. At Dayton he founded the Nano-Fabrication Laboratory for optical thin films, interference lithography and semiconductor processing.

Keigo Hirakawa is an Assistant Professor in the Electrical and Computer Engineering at the University of Dayton, Dayton, Ohio. He founded the Intelligent Signal Systems Laboratory which focuses on research in statistical signal processing, image processing, and computer vision. He received his B.S. in Electrical Engineering from Princeton University in 2000, M.S. and PhD in Electrical and Computer Engineering from Cornell University in 2003 and 2005, respectively, and M.M. in Jazz Performance from New England Conservatory in 2006. Before the University of Dayton, he was a Research Associate at the Harvard University.